JOURNAL OF APPLIED ELECTROCHEMISTRY **27** (1997) 396–403

Electrochemical and ellipsometric study of the oxide films formed on copper in borax solution Part II: Effect of ozone

M. F. L. DE MELE, M. R. VIERA, J. O. ZERBINO

Instituto de Investigaciones Fisicoquímicas Teóricas y Aplicadas (INIFTA), Facultad de Ciencias Exactas, Universidad Nacional de La Plata, Sucursal 4, Casilla de Correo 16, (1900) La Plata, Argentina

Received 10 January 1996; revised 3 July 1996

The influence of O_3 on the passive behaviour of copper was analysed in the potential region −0.32 to 0.70 V vs RHE in borax solutions (pH 9.2) through voltammetric techniques and ellipsometry. Oxide formation can be explained as a sequence of Cu_2O growth, Cu(II) chemisorption, and dissolution precipitation steps similar to those corresponding to copper electrodes in deaerated solutions. The role of Cu(II) chemisorption is discussed in this paper. The progressive accumulation of hydrated layers hinders the reaction between O_3 and the metal. O_2 and O_3 promote growth and dissolution processes (both at open circuit and in controlled potential experiments) but O_3 has a stronger effect.

1. Introduction

The growth of microorganisms and biofouling constitute a large problem in cooling water systems because of the tendency to use alkaline treatments. Biofouling of cooling water equipment causes several difficulties such as the acceleration of corrosion of many engineering alloys, the reduction in the efficiency of heat transfer, the decrease in water flow rate and the increase of pathogenic organisms in weakly alkaline solutions [1].

Biocorrosion and biofouling are usually controlled by biocides such as chlorine or hypochlorite in industrial systems. However, the use of dissolved chlorine causes high corrosivity to several alloys, storage difficulties and environmental damage [2].

The effectiveness of O_3 in the prevention of microorganism growth has been claimed for many years. O_3 is easily generated from pure O_2 or air, it is nontoxic to human beings at the levels required to control microorganism growth and it does not require storage capacity. This powerful oxidizing agent may cause corrosion problems on metals. O_3 at levels above 0.2 ppm increases corrosion in several alloys [3]. However, few reports have been published concerning the O_3 effect on metallic corrosion [2–5].

Corrosion product films, dense and adherent, inhibit the corrosion of copper alloys in quasi neutral aqueous solutions. Studies performed in deaerated solutions showed that the passive film presents a duplex structure in which Cu_2O, CuO or $Cu(OH)_2$ may be present depending on the formation conditions [6–9]. A high O_3 concentration probably hinders the growth of the protective layer [10]. Differences in the colour of corrosion products formed on naval brass were observed between ozonated and aerated solutions [2]. Golden corrosion products were found in ozonated solutions whereas whitish green products were found in aerated solutions. Therefore, the influence of O_3 on the copper oxide formation is interesting from both the fundamental and practical points of view.

Potentiodynamic programmes and cyclic voltammetry complemented with ellipsometry were used in this work to characterize *in situ* the oxide formation in ozonated solutions. Comparative experiments carried out in solutions saturated with O_2 and N_2 are also reported. The dissolution process is particularly analysed.

2. Experimental details

Experiments were made at room temperature in saturated solutions bubbling either N_2 (sol I), O_2 (sol II) or O_2/O_3 (sol III). O_3 was produced through a flux of O_2 in contact with a xenon lamp which was supplied by a 3 kV source (Dinavox). Dissolved O_3 solutions up to 1 ppm concentration were obtained by bubbling the O_2/O_3 mixture in the cell. The O_3 concentration was measured using the indigo trisulfonate method. Experimental conditions were similar to those described in previous publications [8, 11]. The grain size of the electrode was estimated as about 10 μm through optical microscopy and STM measurements [12]. The tested optical area was about 1 mm^2 and the electrode area 0.4 cm^2.

The ellipsometric parameters of the initial recently polished copper surface, horizontally placed, were obtained at $E_c = -0.32$ V vs RHE. The experimental procedures were the following:

0021-891X

Procedure A: The values of Δ and Ψ at E_c were recorded as a function of time (t).
Procedure B: Δ and Ψ were measured at open circuit potentials (E_{oc}). Then the potential was scanned from E_{oc} up to E_c.
Procedure C_1: Δ and Ψ were recorded at E_c after cycling the potential at 0.10 V s^{-1} at different times (τ) between E_c and E_a (E_a = 0.62 V or 0.72 V).
Procedure C_2: As for C_1 including a potential holding at E_a during a time t into each cycle.
Procedure D: Δ, Ψ, current and potential were recorded simultaneously during a potential sweep at v = 1.5 mV s^{-1}.

3. Results

3.1. *Open circuit experiments*

The evolution of the ellipsometric parameters Δ and Ψ at E_{oc} for a recently polished electrode (procedure B) immersed for 4 h in stirred sol III is represented in Fig. 1(a). Δ decreases and Ψ remains constant or decreases during the first minutes relative to the bare electrode. Then Ψ increases sharply while Δ also increases. After the reduction of the oxide layer at 10 mV s^{-1} the Δ/Ψ relationship measured at E_c differs from that corresponding to the bare electrode. The behaviour at E_{oc} of the electrodes held at E_c (procedure A) depends on time t (t = 3 min, Fig. 1(a) and 30 min, Fig. 1(b)).

Data corresponding to Fig. 1 obtained at E_{oc} are plotted on the left side of Fig. 2 as a function of time. Curves (a) correspond to the optical parameters of Fig. 1(a) and curves (b) to those of Fig. 1(b). The E_{oc} against time dependence was also included in the upper frame. E_{oc} rises during the first minutes attaining a stable value at about 0.68 V. In Fig. 2 $-\delta\Delta$ and $\delta\Psi$ indicate a change of Δ and Ψ related to the bare surface. Initially $-\delta\Delta$ increases up to about 5.5 degrees, then remains constant and after one hour decreases, returning to the initial value (Fig. 2, left). $\delta\Psi$ shows small and negative values during the first minutes and then it increases. Concomitant changes in the slopes of the $-\delta\Delta/t$ and the $\delta\Psi/t$ curves are noted.

Data measured in sol I and sol II [8] are also included in Fig. 2 (right side) to be compared with those of sol III. The arrows show the time when the O_2 bubbling started. The $-\delta\Delta$ maximum value as well as E_{oc} of sol III are higher (Fig. 2 left side, curves (a)) than those corresponding to sol II for the same time (Fig. 2, right side).

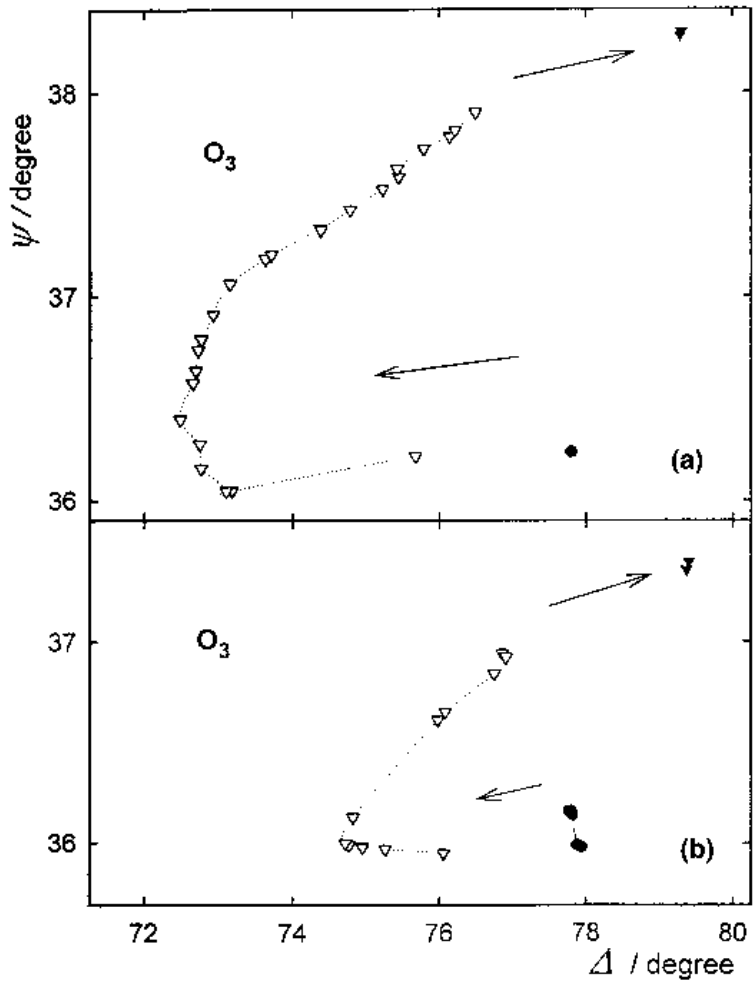

Fig. 1. Ellipsometric plot obtained under O_2/O_3 bubbling during the potential holding at E_c (●): (a) t = 3 min at E_c, (b) t = 30 min at E_c (procedure B), (▽) the evolution at E_{oc} (procedure A) for (a) 4 h and (b) 1 h, and (▼) at E_c after reduction.

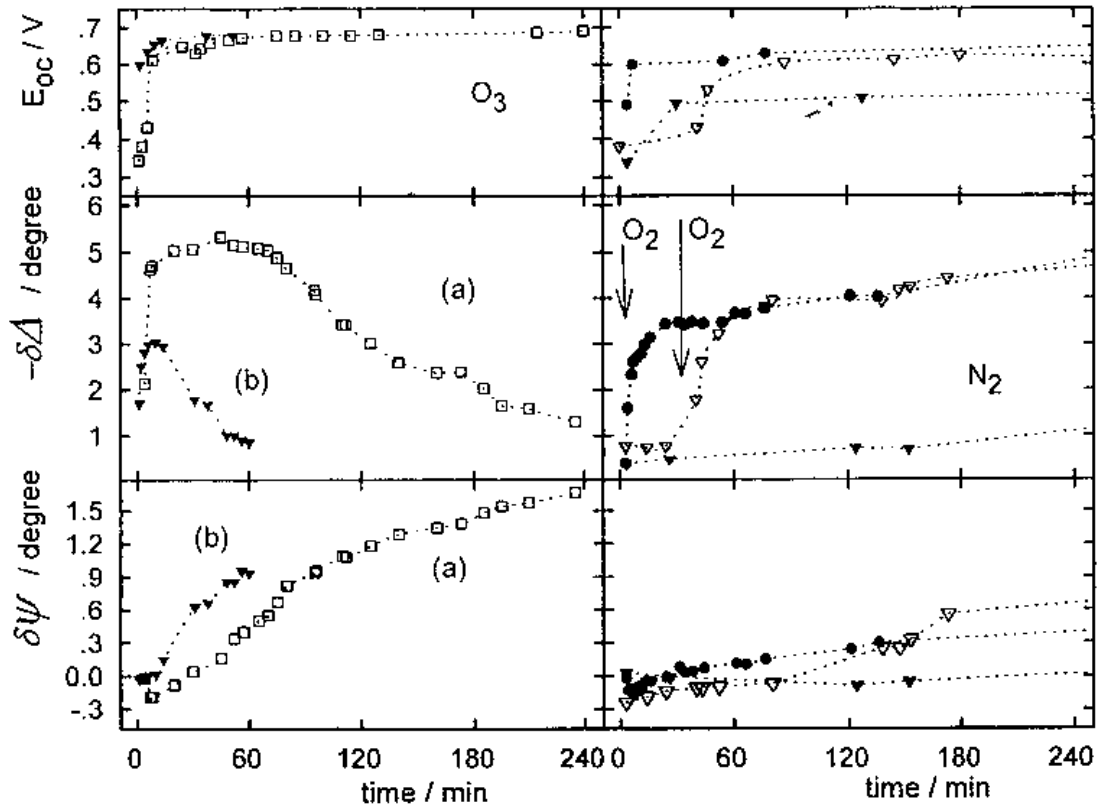

Fig. 2. Dependence of $-\delta\Delta$, $\delta\Psi$ and E_{oc} on time. Plots on the left are related to Fig. 1 data, curve (a) from Fig. 1 a; curve (b) from Fig. 1 (b). Plots on the right were obtained from ref.: [8], Fig. 2.

The change in Ψ at E_{oc} is similar during the first minutes, ($\delta\Psi = -0.2$ degrees) for a fresh electrode immersed in solutions I, II or III. However, in the presence of O_3 , ψ increases sharply after a few minutes at E_{oc}.

3.2. *Potentiodynamic measurements*

Measurements in sol I were carried out to analyse the influence of the potential on the structure of the oxide layers. The E against i plot, obtained according to procedure C_1 at 0.1 V s^{-1} ($E_a = 0.72$ V, Fig. 3(a)), shows three current contributions: at 0.50 V (I*a*), 0.36 V (I*b*) and 0.05 V (I*c*). When cycling time, τ, increases the peak charge decreases. The split of the cathodic peak into two current contributions (I*a* and I*b*, Fig. 3(a)) is more evident if the potential is held at E_a (procedure C_2, Fig. 3(b)). The I*b* peak shifts cathodically from 0.39 to 0.28 V when t increases from 3.5 to 50 s.

Voltammograms obtained after applying procedures C_1 and C_2 show a decrease of the whole cathodic profile when τ increases. However, the decrease in the I*b* peak is more significant than that of the I*a* peak.

3.3. *Ellipsometric measurements at E_c*

Δ/Ψ relationships obtained by carrying out either procedure C_1 (Fig. 4(a), (a′)) related to Fig. 3(a) or procedure C_2 (Fig. 4(b), (b′)) related to Fig. 3(b) show similar initial slopes. The total Δ/Ψ change depends on E_a , t and τ. After a 60 min cycling period Δ/Ψ values are far from those corresponding to the bare electrode (filled circle). With the electrode held at E_a for 50 s the ellipsometric parameters were measured (Fig. 4 (b), (b′), filled triangles). The Δ and Ψ obtained after the reduction process correspond to the filled inverted triangles.

The increase of $\delta\Psi$ with time, measured at E_c (procedure A), for solutions I, II and III is shown in Fig. 5(b). The plots fit a $\delta\Psi$ against square root of time relationship. During potential cycling, in deaerated condition, an increase in Ψ is also observed which depends on the potential E_a and on the cycling time τ (Fig. 4(a′)). For $E_a = 0.72$ V, the $\delta\Psi$ against time dependence is nearly linear (Fig. 5(a)).

3.4. *Δ/Ψ during a potential cycle in solutions I, II and III*

The variation of Δ/Ψ during a potential cycle (procedure D) between E_c and $E_a = 0.68$ V for a recently polished electrode is compared in Fig. 6(a), (b) and (c). In the case of sol I (Fig. 6(c)), Δ reaches a minimum during the cathodic scan and then increases. In the case of sol II and sol III two minima are achieved during the cycle (Fig. 6 (a) and (b)). Δ/E and Ψ/E plots obtained in sol III are shown in Fig. 7. During the anodic scan an increase in Ψ and a sharp decrease in Δ over 0.50 V are observed. Subsequently, Δ increases at 0.62 V. During the cathodic scan Δ attains

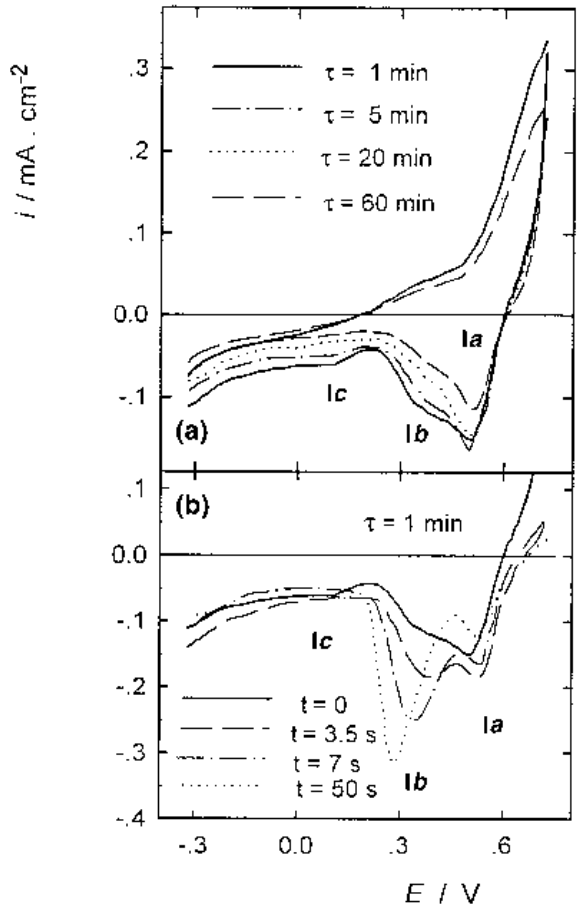

Fig. 3. Potentiodynamic profile after different cycling times τ, at $v = 0.1$ V s^{-1} from $E_c = -0.32$ V to $E_a = 0.72$ V. (a) Procedure C_1.with τ: (——) 1, (–·–·–) 5, (·····) 20 and (– – –) 60 min. (b) Procedure C_2 with cathodic scan after a potential holding during different times, t, at E_a for t: (——) 0, (– – –) 3.5, (–·–·–) 7 and (·····) 50 s.

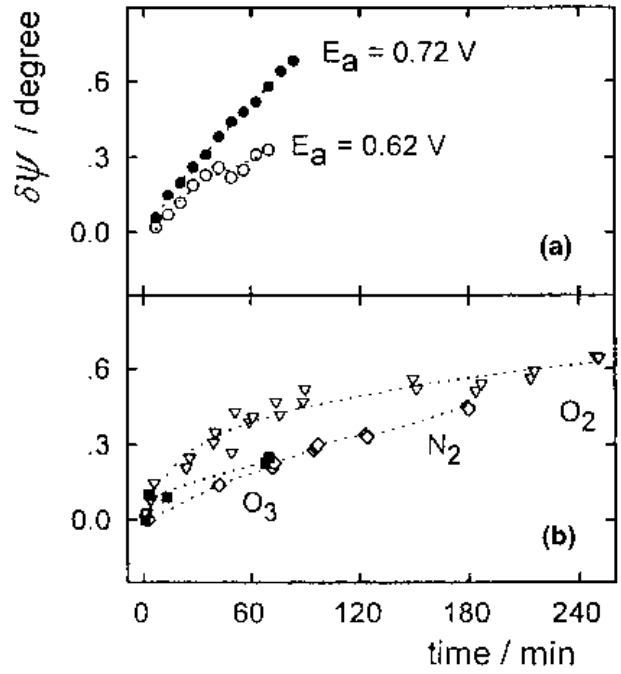

Fig. 5. Evolution of $\delta\Psi$ with time: (a) measured at E_c after cycling from E_c to E_a (procedure C_1) in N_2 saturated solutions; (b) during potential holding at E_c (procedure B) in N_2, O_2 and O_2/O_3 solutions.

a maximum and then a minimum with a concomitant increase and decrease in Ψ. The optical parameters at the end of the experiment are different from those corresponding to the bare electrode (initial value). The comparison with results obtained with sol I and sol II (Fig. 6(b), (c) and in [8], Figs 9 and 10) shows that the irreversible changes are larger in sol III than

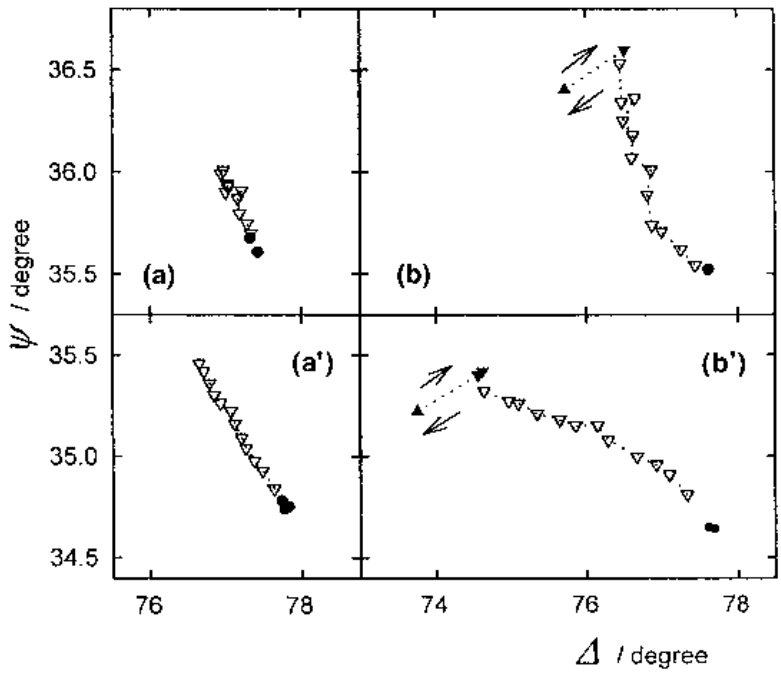

Fig. 4. Ellipsometric data associated to experiments described in Fig. 3 according to: procedure C_1 ((a) and (a′) from Fig. 3(a)); procedure C_2 ((b) (b′) from Fig. 3(b)). (●) at $E_c = -0.32$ V up to $t = 10$ min (procedure B); (▽) at E_c after successive cycling periods of $\tau = 5$ min; (▲) at $E_a = 0.72$ V, $t = 50$ s; (▼) at E_c. Key: (a) 0.62 V; (b) 0.72 V, $t = 7$ s; (a′) 0.72 V, (b′) 0.72 V, $t = 3.5$ s.

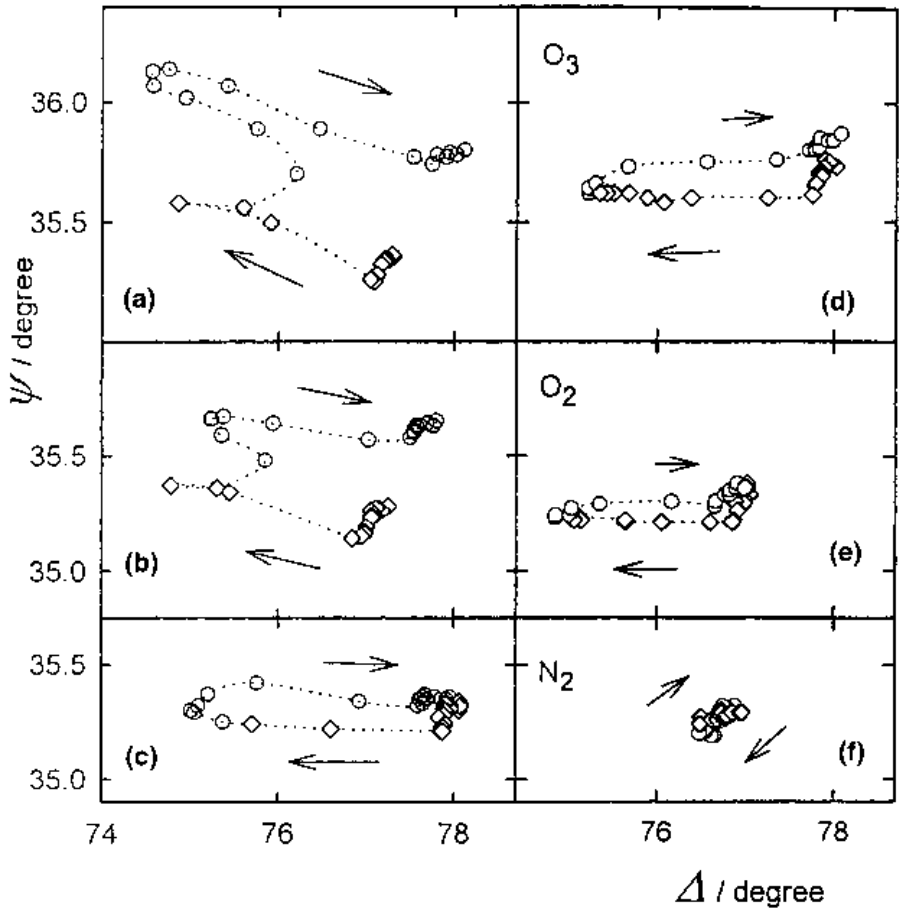

Fig. 6. Comparison of Δ/Ψ values measured during a potentiodynamic cycle at $v = 1.5$ mV s^{-1} (procedure D) between E_c and $E_a = 0.68$ V (left side) and between E_c and $E_a = 0.53$ V followed by a potential holding at E_a for $t = 5$ min (right side). Solutions were saturated with O_2/O_3 (a, d), O_2 (b, e) and N_2 (c, f). (◇) anodic scan, (○) cathodic scan.

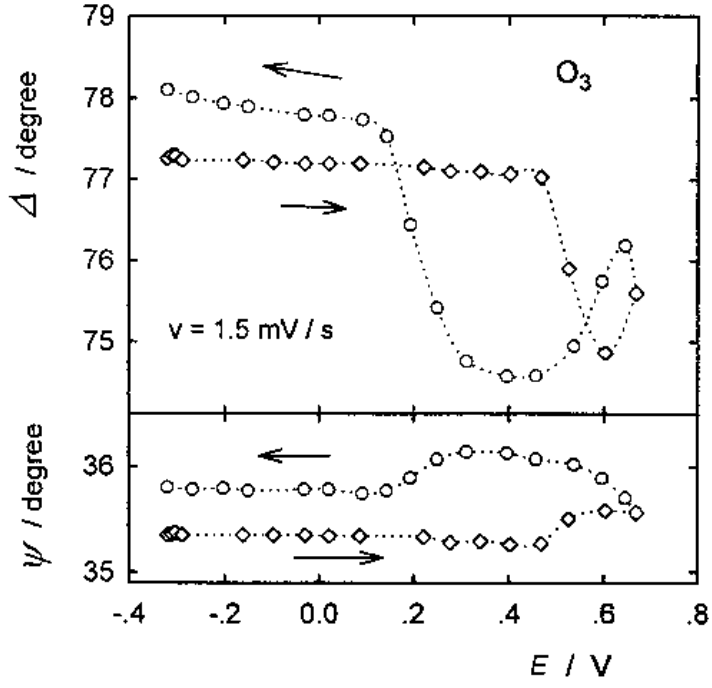

Fig. 7. Δ and Ψ against E data corresponding to a O_2/O_3 solution in the condition described in Fig. 6(a).

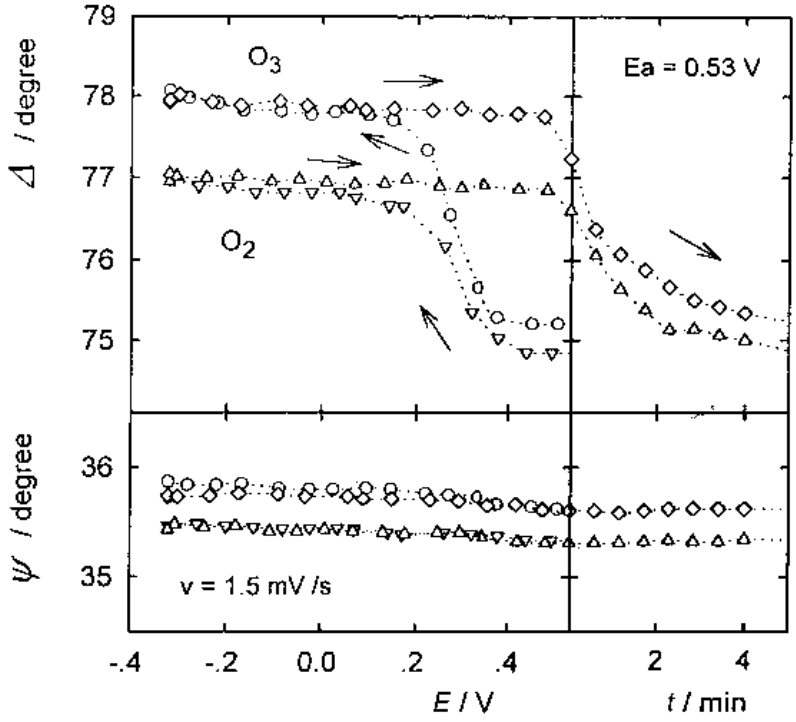

Fig. 8. Δ and Ψ against E data corresponding to O_2 (Δ anodic and ∇ cathodic scan) and O_2/O_3 saturated solutions ($\diamond$ anodic and $\circ$ cathodic scan) for the scan programme described in Fig. 6 (e) and (d). The transients at E_a were included on the right frames.

in sol I and sol II and take place at potentials more anodic than 0.53 V.

Fig. 6(d), (e) and (f) and Fig. 8 show Δ and Ψ against E relationships. These were obtained during a potential cycle where a 5 min potential holding at $E_a = 0.53$ V was included. The changes in Δ and Ψ during the cycle in sol I are reversible and lower than 0.6 degrees (Fig. 6 (f)). In contrast, Δ/E and Ψ/E relationships for sol II and sol III show larger changes (Fig. 8). The higher variations of the optical parameters correspond to sol III (Fig. 6 (d)) where an irreversible change of Ψ occurs.

During the anodic scan, from E_c to $E = 0.5$ V, a decrease of about 0.15 degrees in Ψ and Δ is observed (Fig. 8). At higher potentials the Δ/Ψ slope changes, decreasing Δ more than 2 degrees while Ψ remains constant (Fig. 6 (d) and (e)). During the cathodic scan a similar change of the Δ/Ψ slope results below 0.15 V (Figs 6 and 8).

4. Discussion

According to [8], copper electrodes developed a complex Cu/Cu_2O/electrolyte interface in aerated and deaerated borax solutions. An *inner* Cu_2O dehydrated *passivating layer* adjacent to the metal (ippl) and an *outer* hydrated *layer* of $Cu(OH)_2$ (oppl) was found in weakly acid or alkaline solutions [6–8, 13]. A linear (region I) or a parabolic (region II) growth of the ippl up to a limiting thickness followed by a dissolution precipitation process (region III) was demonstrated. The ippl was composed of Cu_2O with a surface excess of Cu(II) ions. The thickness of the layers depended on the potential, time and stirring conditions. O_2 increased the growth of either the ippl or the oppl depending on the electrode potential [8]. Experiments performed in the presence of O_3 provided more experimental evidence to evaluate corrosion problems when O_3 was used as biocide and to attain a mechanistic approach to the copper/water interfacial processes.

4.1. *Inner layer* (*ippl*)

$-\delta\Delta$ can be considered as proportional to the thickness of the ippl [8, 11, 14, 15]. The ippl grew linearly (at $E_{oc} < 0.53$ V) or parabolically (at $E_{oc} > 0.53$ V) with time under the oppl (Fig. 2). After a potential cycling of $\tau = 60$ min the anodization at $E_a = 0.72$ V and the reduction at E_c produced a quasi reversible change in Δ (Fig. 4 (b), (b′), see arrows). The Δ and Ψ changes between E_c and E_a resulted independent of the previously applied cycling programme. This indicates the growth of an ippl between the metal and the oppl similar to that formed on recently polished electrodes [8].

A decrease in roughness of the interfacial film and a limiting thickness was reported in the case of thinner layers produced by oxidation of copper in the gaseous phase [16] indicating preferential oxidation of the apexes. In sol II at E_{oc}, the detachment of some oxide particles may be hindered and the corrosion controlled due to the oxidation front generated [8, 17]. The charge of I*a* peak, related to the contribution of chemisorbed Cu(II) species, remained constant for different times at E_a (Fig. 3) whereas I*b*

peak, related to Cu_2O, shifted cathodically and the charge increased. This reduction profile was similar to that recorded after 24 h at E_{oc} in sol I [8] indicating analogous structures of the ippl, though the charges involved were 10 times higher in the last case.

Voltammograms obtained after 3 h at E_{oc} in sol II and sol III (not included) showed one peak whereas over 24 h they showed two peaks [8]. However, Δ decreased after 10 h in contact with sol III. These results indicate the growth of Cu_2O under the oppl. A thick and compact oppl hinders the diffusion of O_3 to the electrode and then the ippl grows. The larger differences between sol II and sol III in the dark were observed with recently polished electrodes; in contrast, light promoted the dissolution of the ippl even in the case of thick films [18].

The Cu_2O layer that grows under the oppl may incorporate hydrated Cu(II) ions. Therefore, the larger decrease of the I*b* peak relative to the I*a* peak (Fig. 3 (a)) may indicate the formation of a more porous ippl including more hydrated species or chemisorbed Cu(II). This ippl is easily reduced at more anodic potentials. In sol III high E_{oc} values are achieved, the ippl is dissolved and the electrode is covered by a thick oppl (Fig. 2). However, at E_{oc} , for times longer than 240 min, the ippl grows probably consuming the oppl which hinders the O_3 diffusion.

4.2. *Hydrated outer layer* (*oppl*)

Copper has the larger stability at pH 9.2 [19] showing the greatest precipitation of soluble species at this pH. The total quantity of deposited hydrated oxide can be estimated through the change in Ψ [8, 14]. The oppl, associated with the $\delta\Psi$ increase can be formed either by potential cycling (Fig. 4), by an anodic (E_a) potential holding [8], or by a cathodic (E_c) potential holding (Figs 1(b) and 4).

The formation of $Cu(OH)_2$ layers at potentials higher than 0.6 V vs RHE has been reported [6–8, 13]. At potentials higher than 0.00 V vs SCE, $Cu(OH)_2$ formation (in 0.1 M LiOH) was explained by a CuO dissolution precipitation mechanism and by the accumulation of majority carriers. The thermodynamically stable phase CuO was formed at sufficiently low crystallization rates whereas the formation of $Cu(OH)_2$ prevailed at higher rates [20].

4.2.1. Dissolution process at $E < 0.62$ V. Hultquist [21] measured an average weight gain of 0.11 μg cm^{-2} h^{-1} for copper samples at low potentials immersed in distilled water. He concluded that copper is oxidized by water. The escape rate of hydrogen was considered of decisive importance for the corrosion kinetics of copper. In agreement, present results show the growth of the oppl at low potentials.

At E_c the oppl growth rate in stirred solutions I, II or III was similar (Fig. 5(b)). The $\delta\Psi$ against square root of time dependences indicate that the growth of the oppl occurs under diffusion control.

Ψ increases in stirred aerated borax solutions rather than in stagnant solution [8]. This suggests a larger dissolution and precipitation of Cu(II) in the former case. On the other hand, in pure oxygenated water the time required to saturate the interface was longer under stirring. A Ψ increase was detected after 90 min at E_{oc}. Through X-ray diffraction this change was analysed and was attributed to the growth of a new Cu(II) oxide layer [15].

It is important to mention that copper was used in microcapsulation methods to improve the thermal conductivities and hence the kinetics of the hydrogen absorption [22]. The performance of copper powder as bonding material was not good enough and graphite seemed to have a better behaviour in hydride electrodes [23]. The present results suggest that this lower efficiency can be attributed to the formation of the oppl even at cathodic potentials [19].

4.2.2. Dissolution process at $E > 0.62$ V. Similar $\delta\Psi$ against time dependences are obtained by cycling the electrode between $E_c = -0.32$ V and $E_a = 0.62$ V in sol I (Fig. 5(a)) and by a potential holding at E_c (Fig. 5(b)). The corresponding i/E voltammogram shows I*b* and I*c* peaks involving a charge of 162 μC cm^{-2}. For $E_a = 0.72$ V (region III) I*a* peak appears (Fig. 3(a)) increasing the charge associated to each cycle (428 μC cm^{-2}), results in a linear $\delta\Psi$ against time relationship . When E_a is increased from 0.62 to 0.72 V the reduction of the ippl is favoured by Cu(II) chemisorbed (Fig. 3, I*a* peak). However, this Cu(II) is not totally reduced during cycling; but hydrates, increasing the thickness of the oppl (Fig. 5(a)).

Δ/Ψ values obtained after reduction (Fig. 1, filled inverted triangles) indicate that the oppl remains on the surface after reduction of the ippl [14]; roughness increase may be disregarded [8] suggesting that in sol III the dissolution process proceeds as a smooth oxidation front.

The different Δ/Ψ slopes observed in Fig. 4 ((b), (b′)) can be explained assuming different thickness of the initially formed oppl. The oppl becomes more compact during the successive dissolution precipitation processes [14]. The decrease of the current during the cycling time τ (Fig. 3(a)) indicates an increasing barrier effect of the oppl on the growth of the ippl during cycling.

The ippl formed in sol I was reduced at potentials more cathodic than that formed in sol II [8]. In the case of sol III the reduction profile after procedure B (not shown) had a smaller current contribution at low potentials than that of sol II. This fact may be attributed to a more anodic interfacial potential and a higher hole concentration, which probably increases the amount of Cu(II) adatoms and accelerates the dissolution process.

If the oxidation of Cu to Cu_2O proceeds by a hole mechanism, the accumulation of holes in Cu_2O is required for the oxidation process and likewise a depletion condition is necessary for the ippl reduction

[20]. The flat band potential (E_{fb}) corresponds to the potential of the Cu/ Cu_2O couple. The dissolution of CuO is explained by the degenerate surface that accompanies the accumulation of majority carriers at potentials more anodic than E_{fb} [20].

The present results confirm those previously reported in sol I and sol II [8]. The chemisorption of Cu(II) ions can bend the bands and hinder the growth of the Cu_2O layer. The shift in the Fermi level and the deflect of the holes near the metal may also accelerate the reduction and the dissolution process.

4.3. *Effect of O_2 and O_3 at controlled potential and at E_{oc}*

O_3 is a strong oxidizer (redox potential of 2.07 vs SHE). The E_{oc} in the presence of O_3 shifts to more anodic values than in sol I and II reaching 0.680 V (Fig. 2(a)). This potential is near to those corresponding to the Cu_2O/CuO equilibria of the dehydrated and hydrated CuO (0.669 V and 0.747 V, respectively). In sol I, E_{oc} attains potential values associated to Cu_2O formation (region I). Therefore, the presence of O_2 and O_3 promotes the growth of the ippl at potentials lower than 0.53 V (Fig. 6 (a), (b), (c)) and the dissolution process at higher potentials (Fig. 4 (d), (e), (f)). Previously reported data in pure water stated that the value of the limiting thickness probably depended on the ability of electrons and ions to get through the oxide film and react at the surface [15]. Sufficient electrons are available to reduce Cu(II) to Cu(I) below the limiting thickness, and the film thickness increases.

Though the sequence of the processes occurring in solutions I, II and III is similar [8], the potential regions shift cathodically in sol II and sol III. This is more evident in the last case (Fig. 6).

OH^- radicals were reported in the reduction of O_3 in water [2]. Probably, sol II and sol III supply oxidizing intermediates which increase the concentration of chemisorbed Cu(II) species and the electron hole transport (region II). Then, according to the potential, they promote the growth of the dehydrated oxide layer or the dissolution precipitation process (Figs 2 and 5) shifting cathodically the potential limits of regions II and III.

5. Conclusions

Maximal Cu(II) adsorption can be induced either by a chemical reaction with water (transition from region I to II) or by high anodic potential values (transition from region II to III). The chemisorption of Cu(II) ions may hinder the growth of the ippl and accelerate the dissolution process. The presence of O_3 promotes, at $E_{oc} < 0.53$ V (first minutes of immersion), the growth of the ippl on bare electrodes. O_3 increases the dissolution process at higher potentials and consequently the oppl thickness. Corrosion of copper is favoured in this condition. The oppl grows even at cathodic potentials and works as an effective barrier for the O_3 diffusion.

Acknowledgements

This work was supported by the Consejo Nacional de Investigaciones Científicas, the Comisión de Investigaciones Científicas de la Provincia de Buenos Aires (CIC) and Fundación Antorchas. J. O. Z. and M. F. L. de M. are members of the Research Career of CIC and CONICET respectively. The authors are very grateful to Dinavox for the supply of the ozone generator.

References

[1] D. H. Pope, L. W. Eicheler, T. F. Coates, J. F. Kramer and R. J. Soracco, *Current Microbiology* **10** (1984) 89.
[2] B. E. Brown and D. J. Duquette, 'A review of the effects of dissolved ozone on the corrosion behavior of metals and alloy'. Corrosion'94 (1994) paper 486, Houston, TX
[3] S. Hettiarachchi, 'The effect of ozone on corrosion of steel and copper in cooling water systems'. Corrosion'91 (1991) paper 206, NACE, Houston, TX.
[4] M. Matsudaira, M. Susuki and Y. Sato, *Mater. Performance* **11** (1981) 55.
[5] H. H. Lu and D. J. Duquette, *Corrosion* **46** (1990) 10.
[6] H. H. Strehblow and B. Titze, *Electrochim. Acta* **25** (1980) 839.
[7] H. H. Strehblow and H. D. Speckmann, *Werkst. Korros.* **35** (1984) 512.
[8] J. O. Zerbino and M. F. L. de Mele. *J. Appl Electrochem*, in press.
[9] J. M. Brooke and P. R. Puckorius. 'Ozone for cooling tower system is it a panacea' Corrosion'91 (1991) paper 212, NACE, Houston, TX.
[10] B. Yang, D. A. Johnson and S. H. Shim, *Corrosion* **49** (1993) 499.
[11] M. R. Gennero de Chialvo, J. O. Zerbino, S. L. Marchiano and A. J. Arvia, *J. Appl. Electrochem.* **16** (1986) 517.
[12] S. G. Aziz, G. Andreasen, M. E. Vela, R. C. Salvarezza and A. J. Arvia, in preparation.
[13] N. S. McIntyre, S. Sunder, D. W. Shoesmith and F. W. Stanchell, *J. Vac. Sci. Technol.* **18** (1981) 714.
[14] O. A. Albani, L. M. Gassa, J. O. Zerbino, J. R. Vilche and A. J. Arvia, *Electrochim. Acta* **35** (9) (1990) 1437.
[15] J. Kruger and J. P. Calvert, *J. Electrochem. Soc*. **111** (1964) 1038; *idem*., *ibid.* **108** (1961) 503.
[16] T. N. Rhodin, *'Advances in Catalysis*', vol. 4, Academic Press, New York (1953).
[17] M. Moliere, Y. Verdier and C. Leymonie, *Corros. Sci.* **30**(2/3) (1990) 183.
[18] J. Kruger, *J. Appl. Phys*. **28** (1957) 1212.
[19] M. Pourbaix (ed.), *'Atlas of Electrochemical Equilibria*', Pergamon Press, Cebelcor, Brussels, (1966).
[20] S. M. Wilheim, Y. Tanizawa, Chang-Yi Liu and N. Hackerman, *Corros. Sci.* **22** (1982) 791.
[21] G. Hultquist, *ibid*. **26** (1986) 173.
[22] T. Sakai, H. Ishikawa, K. Oguro, C. Iwakura and H. Yoneyama, *J. Electrochem. Soc*. **134** (1987) 558.
[23] A. Visintin, A. Tori, W. E. Triaca and A. J. Arvia, *J. Power Sources*, in preparation.